Remote Sens. **2015**, *7*, 13251-13272; doi:10.3390/rs71013251

OPEN ACCESS

remote sensing

ISSN 2072-4292

www.mdpi.com/journal/remotesensing

Article

Combined Multi-Temporal Optical and Radar Parameters for Estimating LAI and Biomass in Winter Wheat Using HJ and RADARSAR-2 Data

Xiuliang Jin [1,2,3], Guijun Yang [1,2,4,*], Xingang Xu [1,2,5], Hao Yang [1,2], Haikuan Feng [1,2], Zhenhai Li [1,2], Jiaxiao Shen [1,2] Chunjiang Zhao [1,2,4,5] and Yubin Lan [6]

1 Beijing Research Center for Information Technology in Agriculture, Beijing Academy of Agriculture and Forestry Sciences, Beijing 10097, China; E-Mails: jinxiuliang@iga.ac.cn (X.J.); xxg2007@aliyun.com (X.X.); younghow@163.com (H.Y.); fenghk@nercita.org.cn (H.F.); lizh323@126.com (Z.L.); shenjiaxiao@163.com (J.S.); zhaocj@nercita.org.cn (C.Z.)

2 National Engineering Research Center for Information Technology in Agriculture, Beijing 100097, China

3 Key Laboratory of Wetland Ecology and Environment, Northeast Institute of Geography and Agroecology, Chinese Academy of Sciences, Changchun 130102, China

4 Key Laboratory for Information Technologies in Agriculture, the Ministry of Agriculture, Beijing 10097, China

5 Beijing Engineering Research Center of Agricultural Internet of Things, Beijing 100097, China

6 College of Engineering, South China Agricultural University, Guangzhou 510642, China; E-Mail: lanyubin@gmail.com

* Author to whom correspondence should be addressed; E-Mail: guijun.yang@163.com; Tel.: +86-10-51-503-647; Fax: +86-10-51-503-750.

Academic Editors: Nicolas Baghdadi and Prasad S. Thenkabail

Received: 21 August 2015 / Accepted: 29 September 2015 / Published: 6 October 2015

Abstract: Leaf area index (LAI) and biomass are frequently used target variables for agricultural and ecological remote sensing applications. Ground measurements of winter wheat LAI and biomass were made from March to May 2014 in the Yangling district, Shaanxi, Northwest China. The corresponding remotely sensed data were obtained from the earth-observation satellites Huanjing (HJ) and RADARSAT-2. The objectives of this study were (1) to investigate the relationships of LAI and biomass with several optical spectral vegetation indices (OSVIs) and radar polarimetric parameters (RPPs), (2) to estimate LAI and biomass with combined OSVIs and RPPs (the product of OSVIs and RPPs (COSVI-RPPs)), (3) to use multiple stepwise regression (MSR) and partial least

squares regression (PLSR) to test and compare the estimations of LAI and biomass in winter wheat, respectively. The results showed that LAI and biomass were highly correlated with several OSVIs (the enhanced vegetation index (EVI) and modified triangular vegetation index 2 (MTVI2)) and RPPs (the radar vegetation index (RVI) and double-bounce eigenvalue relative difference (DERD)). The product of MTVI2 and DERD (R^2 = 0.67 and RMSE = 0.68, $p < 0.01$) and that of MTVI2 and RVI (R^2 = 0. 68 and RMSE = 0.65, $p < 0.01$) were strongly related to LAI, and the product of the optimized soil adjusted vegetation index (OSAVI) and DERD (R^2 = 0.79 and RMSE = 148.65 g/m^2, $p < 0.01$) and that of EVI and RVI (R^2 = 0. 80 and RMSE = 146.33 g/m^2, $p < 0.01$) were highly correlated with biomass. The estimation accuracy of LAI and biomass was better using the COSVI-RPPs than using the OSVIs and RPPs alone. The results revealed that the PLSR regression equation better estimated LAI and biomass than the MSR regression equation based on all the COSVI-RPPs, OSVIs, and RPPs. Our results indicated that the COSVI-RPPs can be used to robustly estimate LAI and biomass. This study may provide a guideline for improving the estimations of LAI and biomass of winter wheat using multisource remote sensing data.

Keywords: optical spectral vegetation indices; radar polarimetric parameters; LAI; biomass; winter wheat

1. Introduction

Accurate estimation of crop biophysical and biochemical parameters during crop growing season is important for improving crop field management [1]. Two important indicators of these parameters-leaf area index (LAI) and above ground biomass (AGB)-were used to monitor crop canopy structural development and growth changes and to estimate yield. The reasonable and reliable estimation of LAI and biomass can improve crop fertilizer applications [2], water irrigation [3,4], disease and weed control [5,6], and grain production marketing [7–9]. LAI and biomass change seasonally under different environmental conditions, and therefore, it is important to timely estimate their values. These parameters are traditionally estimated through destructive, time-consuming *in situ* methods, which are difficult to conduct when crops cover large regions.

Owing to its capacity to obtain information on global and regional scales, remote sensing has become an effective tool for estimating LAI and biomass over large areas. Crop canopy structure mainly affects the spectral reflectance of crop canopy in the near-infrared (NIR) and visible spectrums. Numerous studies have shown a strong correlation between vegetation indices (VIs) and LAI and biomass using different integrations of visible and NIR reflectance [10–17]. A previous study has shown that normalized difference vegetation index (NDVI) was very sensitive to low LAI values (*i.e.*, LAI < 3) and saturation exists at medium to high LAI values (*i.e.*, LAI > 3) [16]. Similarly, the saturation of NDVI values was shown at medium to high values of fresh biomass (around 2000 g/m^2) [13]. The simple ratio [16], the modified triangular vegetation index 2 (MTVI2) [18], and the cumulative MTVI2 [19] have shown better sensitivity at medium to high LAI and biomass. Previous results have

shown that VIs based on the reflectance of red-edge bands (e.g., the red-edge triangular vegetation index (RTVI) and the modified chlorophyll absorption ratio index (MCARI2)) have great potential for improving estimations of LAI and biomass [13,18]. Most VIs have mainly been derived from field spectral radiometers [16,17,20], airborne spectrographic imagers [18], medium resolution spectrometers [20], and high-resolution spectrometers [21]. However, optical satellite images often have some limitations with respect to VIs because of the saturation problem and the subsequent reduction in estimation accuracy at medium to high LAI and biomass [13–17,22].

Compared with optical satellite images, synthetic aperture radars (SARs) have some advantages for monitoring crop growth status at medium to high LAI and biomass owing to the fact that microwave sensors have longer wavelengths, can penetrate crop canopies, and are not influenced by the presence of clouds or haze [23]. However, SAR images are limited by the technique's imaging geometry and radiation mechanism [24]. Several SARs have been launched, such as ALOS-PALSAR (Japan), TerraSAR-X (Germany), Sentinel 1 (European Space Agency), and Radarsat1 and 2 (Canada). Some SARs have a short revisit time and high spatial resolution, which could be beneficial for monitoring crop development and health status [25,26]. Many studies have estimated LAI and biomass based on SAR images data acquired from either airborne or space-borne platforms [27–31]. Some studies have shown that SAR backscattering was well correlated with biomass, especially that characterized by medium fractional cover [32–34]. Since optical and SAR image data respond to crop characteristics differently, their complementary information content can support the estimation of crop conditions [12]. The combination of optical and SAR image data has been used for the estimation of the LAI and biomass of crops and forests, and the results have shown that the estimated values agree well with the actual values [27,35–37]. Gao *et al.* estimated the LAI, height, and biomass of maize using single-temporal environment and disaster monitoring satellite constellation (Huanjing (HJ)-1A/B) and RADARSAT-2; the results showed that this integrated method of determining VIs were well correlated with the LAI, height, and biomass near the maize heading stage [24]. However, few studies have combined the optical and SAR data based on multi-temporal images for estimating the LAI and biomass of winter wheat.

Winter wheat is a main crop in Shaanxi Province. The accurate estimation of LAI and biomass for this crop is important for agricultural management and production in this region. HJ-1A/B data provides ground surface spectral information at a 30-m spatial resolution with a two-day revisit frequency (see Section 2.3.1). Compared with other satellite data, HJ-1A/B data is a very good solution to balance the problems of spatial and temporal resolution. Thus, the HJ-A/B data with high spatial and temporal resolutions can offer an opportunity to monitor winter wheat growth status efficiently and objectively over large areas. In this study, the integration of high resolution SAR (RADARSAT-2) and optical image data (HJ-A/B) based on multi-temporal images data was further used to boost the estimation power of the LAI and biomass of winter wheat without adding to the concept of optical-SAR fusion. The major objectives of this study were the following: (i) to investigate the relationships of LAI and biomass with several optical spectral vegetation indices (OSVIs) and radar polarimetric parameters (RPPs), (ii) to estimate LAI and biomass with combined OSVIs and RPPs (the product of OSVIs and RPPs (COSVI-RPPs)), and (iii) to test and compare multiple stepwise regression (MSR) and partial least squares regression (PLSR) methods for estimating and improving

the estimation accuracy of LAI and biomass of winter wheat based on the OSVIs, RPPs, and COSVI-RPPs. This study provides a good guideline for winter wheat field management.

2. Materials and Methods

2.1. Study Area

The field measurements were conducted in the Yangling district (34°2′25″–34°7′23″N, 107°5′10″–108°9′23″E) of Shaanxi, China (Figure 1). The Yangling district covers an area of 22.12 km^2. It is characterized by a typical continental climate and belongs to the semi-arid region of China. The maximum temperature is 26.1°C in the summer, and the minimum temperature is −1.2 °C in the winter. In all the seasons, these climates experience extensive and rapid daily temperature changes, and the temperature difference between day and night is significant. The average annual precipitation is 635.1 mm and the frost-free period is 211 d on average. Three local wheat cultivars (Xinong9871, Shanbei139, and Xiaoyan22) were planted between 5 October and 12 October 2013. The field management followed the local standard practices (weed control, pest management, and fertilizer application) for wheat production.

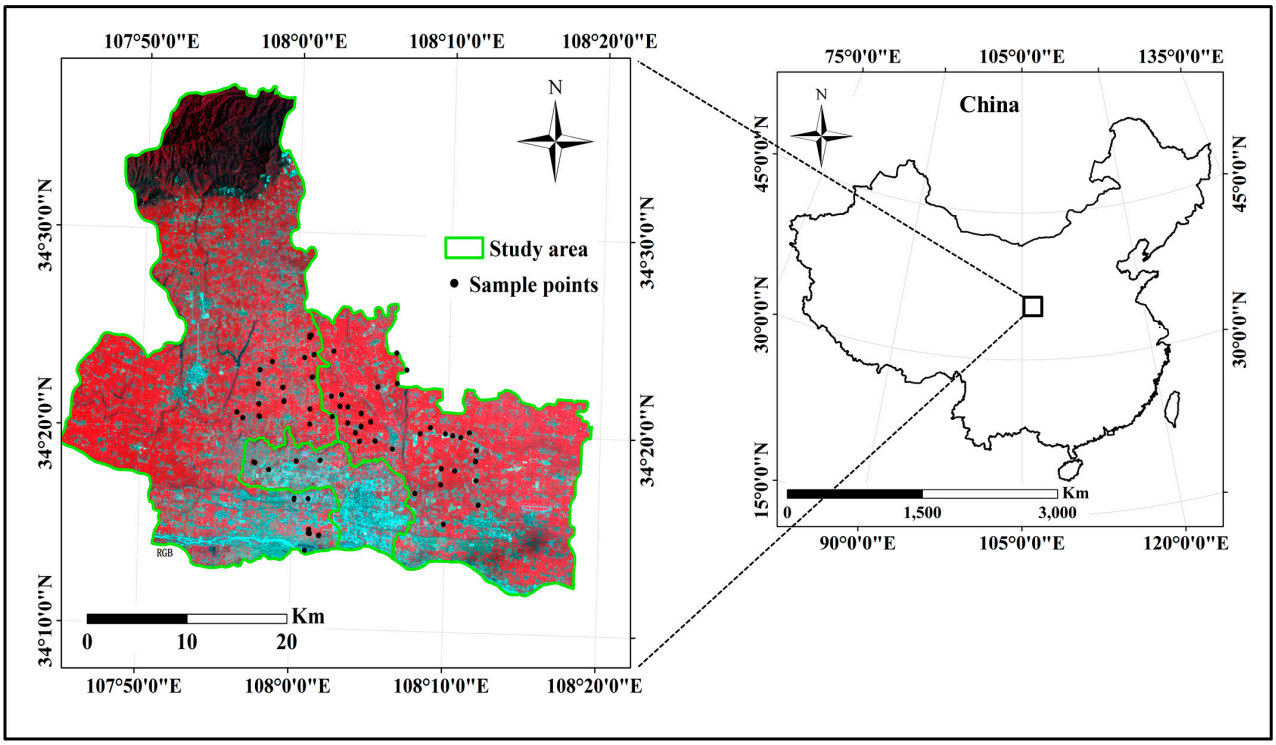

Figure 1. The location map of the study area in Shaanxi, China (False color composite HJ image, acquired on 28 April 2014, R/G/B *vs.* band4/band3/band2).

2.2. Field Data Measurements

The field values of LAI and biomass of winter wheat used in the study was measured from 4 March to 18 May 2014. Table 1 shows the date and number of samples collected during the growing season of winter wheat. In addition, to present the weather conditions during the in-situ field investigation, the

corresponding maximum temperature, minimum temperature, precipitation, relative humidity, and wind speed were recorded at nearby weather stations (Table 1). These data were obtained from the China Meteorological Data Sharing Service System (CMDSSS, http://cdc.cma.gov.cn). In this study, a sample plot area of >20,000 m² stands for one plot. The latitude and longitude of each plot were obtained with Global Positioning System (GPS, Trimble GeoExplorer 2008 Series GeoXH, Trimble Navigation Limited, USA) measurements.

Table 1. Weather conditions and number of samples collected during the in-situ field investigation.

Date of Samples	Maximum Temperature (°C)	Minimum Temperature (°C)	Precipitation per 24 h (mm)	Relative Humidity (%)	Wind Speed (m/s)	Number of Samples
4 March 2014	13.8	5.0	0	52	1.7	30
5 March 2014	7.4	3.1	1.1	66	1.6	
28 March 2014	20.9	9.6	0	68	1.3	30
29 March 2014	23.0	9.7	0	56	1.6	
27 April 2014	21.6	7.9	0	60	1.0	30
28 April 2014	23.8	8.9	0	64	1.5	
14 May 2014	20.6	14.4	0	67	1.5	
15 May 2014	24.5	12.2	0	54	1.4	
16 May 2014	21.3	13.8	0	67	1.0	30
17 May 2014	25.5	12.3	0	64	0.7	
18 May 2014	27.6	14.3	0	63	1.3	

Measurements for the determination of LAI were taken from 1.5 m × 1.5 m using the LAI-2000 Plant Canopy Analyzer (LI-COR Inc., Lincoln, NE, USA) with five replicates using the five-point sampling method from each plot in the central 30 m × 30 m field (Figure 2). One reference reading above the canopy and four readings beneath it were made in order to determine LAI in winter wheat. Below canopy readings were made along diagonal transects between two rows and averaged. Three view caps were used: 90° masks normal (90° n), parallel to the row (90° p), and a 180° mask normal to the row. The purpose was to hide the operator from the sensor's view, providing, at the same time, the largest possible sampling area, and to determine the effect of canopy heterogeneity on the LAI-2000 sensor readings. The sensor with 90° n and 180° masks was always oriented southwards. Using 90° p, the sensor was oriented to the west in the morning and east in the afternoon. The portion of the view that contained the sun was thereby masked out and the effect of direct sunlight avoided.

The aboveground biomass was determined from a 0.20 m^2 area (105 plants) by randomly cutting the representative plants with five replicates using five-point sampling method from each plot in the central 30 m × 30 m field. All the plant samples were heated to 105 °C and oven dried at 70 °C until a constant weight was achieved, and the final dry weight (DW) of the samples was recorded. The DW was divided by sample area, and then the DW is converted to g/m^2. The LAI and biomass measurements during different growing stages of winter wheat were randomly divided into two parts using SPSS software (16.0, SPSS, Chicago, IBM, USA): a calibration set with 80 samples and a validation set with 40 samples. The statistics of each subset for LAI and biomass in winter wheat were summarized in Table 2.

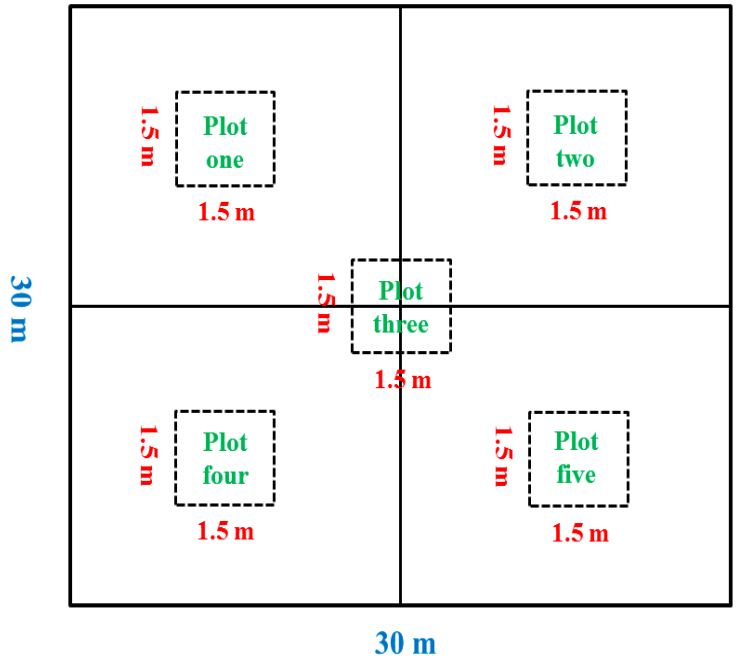

Figure 2. Sampling design using the five point sampling method.

Table 2. Summary statistics of the measured LAI and biomass (g/m^2) of winter wheat in the Yangling district.

Name	Subset	Samples Size	Min	Mean	Max	Range	SD [a]	CV [b] (%)
LAI	Calibration set	80	0.95	3.91	6.95	6.00	1.36	34.78
--	Validation set	40	0.96	3.33	6.14	5.18	1.29	38.73
Biomass	Calibration set	80	73.89	714.67	1711.91	1638.02	400.63	56.06
--	Validation set	40	167.27	723.72	1634.78	1467.51	350.24	48.39

Note: [a]: Standard deviation; [b]: Coefficient of variation.

2.3. Satellite Image Preprocessing

2.3.1. Environment and Disaster Monitoring Satellite Constellation (HuanJing-1A/B)

Images from the environment and disaster monitoring satellite constellation (HuanJing(HJ)-1A/B) that were launched by the China Center for Resources Satellite Data and Applications (CRESDA) on 6 September 2008 were used. The Huanjing CCD image (hereafter referred to as HJ-CCD) had a similar spatial resolution (30 m) and band setting to the widely used Landsat-5 TM. The specific information of HJ-1A/B is shown in Table 3. Compared with the Landsat-5 TM images, the much shorter revisit period of HJ-1A/B (2 days) makes it a good trade-off at both spatial and temporal resolutions. Therefore, HJ-1A/B images were used for monitoring and analyzing the LAI and biomass at key crop growth stages for winter wheat.

The HJ-CCD images were considered for estimating the LAI and biomass from March–May 2014. In order to match the RADARSAT-2 scenes, corresponding 4 HJ-CCD scenes were selected. The detailed scene ID, acquisition time, illumination conditions, path, and row for each scene are given in Table 4. The preprocessing of the HJ-CCD images included radiometric calibration, atmospheric correction, and geometric correction. The calibration coefficients were obtained from the CRESDA

website (http://218.247.138.121/DSSPlatform/index.html). The calibrated data were then atmospherically corrected using the flash model of ENVI 4.7 (ENVI® image processing and analysis software, from ITT Visual Information Solutions, Boulder, CO, USA). One historical Quickbird image with precise geometric correction was used as a reference image. The root mean square error for each geometric-corrected scene was less than one pixel. Each sample plot was corrected by nine pixels to match the ground observations.

Table 3. Detailed information regarding the HJ-1 A/B and RADARSAT-2 satellite images used in the study.

HJ-1 A/B						
Spectral Region (μm)	**Spatial Resolution (m)**	**Orbit Altitude (km)**			**Swath (km)**	
B1: 0.43–0.52 B2: 0.52–0.60 B3: 0.63–0.69 B4: 0.76–0.90	30	649			340	
RADARSAT-2						
Imaging Mode	**Center Frequency**	**Spatial Resolution (m)**	**Mean incidence Angle (°)**	**Orbit Direction**	**Beam Mode**	**Resolution Range × Azimuth (m)**
Fine quad-polarization (HH, HV, VH, VV)	5.405 GHz (C-band)	8	37	Ascend	FQ18	5.2 × 7.2

Note: HH, the normalized radar cross-section (NRCS) measured from the horizontally transmitted and horizontally received signal; VV, the NRCS measured from the vertically transmitted and vertically received signal; HV and VH, the vertically transmitted and horizontally received signal.

Table 4. Detailed information of the acquired Huanjing-1 A/B and RADARSAT-2 satellite images.

Huanjing-1A/B						
Date	**Scene ID**	**Acquisition Time (GMT)**	**Illumination (°)**		**Path**	**Row**
			Sun Zenith	**Sun Azimuth**		
4 March 2014(tillering)	1182664	02:45:12.03	38.679	317.856	15	72
7 April 2014(jointing)	1190156	02:22:15.49	47.867	300.079	7	76
29 April 2014(anthesis)	1200272	02:39:02.22	54.754	297.400	12	72
20 May 2014(filling)	1208502	02:30:07.89	56.114	283.492	8	76
RADARSAT-2						
Date	**Scene ID**	**Acquisition Time (GMT)**	**Illumination (°)**		**Absolute Orbit**	
			Incidence Angle	**Sun Azimuth**		
5 March 2014 (tillering)	313491	10:41:46.789	27.778	349.708	32483.0936	
29 March 2014 (jointing)	317448	10:41:47.153	27.777	349.710	32826.0936	
22 April 2014 (anthesis)	321564	10:41:47.289	27.773	349.709	33169.0936	
16 May 2014 (filling)	325928	10:41:47.413	27.781	349.712	33512.0936	

2.3.2. RADARSAT-2

Four polarization RADARSAT-2 fine quad-pol single-look complex (SLC) images were obtained from March–May 2014. The specific information of RADARSAT-2 is also shown in Table 3. The detailed scene ID, acquisition time, illumination conditions, and absolute orbit for each scene are given

in Table 4. The Radarsat-2 images were processed using PolSARPro version 5.0 (from the European Space Agency) and Alaska Satellite Facility (ASF) Mapready version 3.1. The following specific processing steps were conducted. (1) The Radarsat-2 SLC images were radiometrically calibrated to obtain the linear radar backscattering coefficients (σ°) transformed from the digital number (DN) [38,39] using a look-up table in the product file. (2) A 5 × 5 boxcar filter was used to multi-look and filter for suppressing speckle. (3) The filtered Radarsat-2 images were formed into a scattering matrix (S2), which was then converted to a symmetrized 3 × 3 covariance matrix (C3), which averages the cross-pol backscatter to a single cross-pol value [40,41]. (4) The dataset was ortho-rectified using digital elevation model (DEM)-simulation and registration. The 30 m Advanced Spaceborne Thermal Emission and Reflection Radiometer (ASTER) Global Digital Elevation Model (GDEM) (http://www.gdem.aster.ersdac.or.jp) was used to simulate the SAR image based on its imaging geometry and the available orbit image was matched to the simulated image by warping it to the DEM coordinate system [42,43]. After the terrain correction, the dataset was geocoded into a Universal Transverse Mercator (UTM) map projection. Finally the image was rectified using a preprocessed Quickbird image with a root mean square error of one pixel in geographic position. In order to match the HJ-1A/B image data, the pixel number of the RADARSAT-2 image data was ~144, as each sample plot was corrected by nine pixels to match the ground observations with the HJ-1A/B image data.

2.3.3. Polarization Decomposition Method

The polarization decomposition method, which is considered an effective technique for obtaining polarization and physical features from SAR observations [44], was applied to fully polarimetric SAR data. In this study, two polarization decomposition methods were used to obtain the decomposition parameters: the Freeman-Durden [45] and eigenvalue decomposition methods [46]. The Freeman-Durden method is a decomposition algorithm based on the physical scattering mechanism model. This method divides pixels into three scattering categories: volume scattering (Vol), double-bounce scattering (Dbl), and surface or single-bounce scattering (Odd) according to the dominance of the backscatter power [45]. The total of these parameters (Span) represents the sum of Vol, Dbl, and Odd scattering power. Compared with the Freeman-Durden method, the eigenvalue decomposition method distinguishes the main scattering type and its correlation [46], rather than distributing the energy into three categories. It decomposes the coherency matrix into different eigenvector and eigenvalue set parameters, which are used to describe the scattering mechanisms. The decomposition parameters include three variables: entropy, alpha, and anisotropy. In addition, several eigenvalue set parameters (single-bounce eigenvalue relative difference (SERD) and double-bounce eigenvalue relative difference (DERD)) [47] were selected to analyze the relationships between the decomposition parameters and the LAI and biomass. The eigenvalue decomposition method was applied using PolSARPro version 5.0.

2.4. Radar Polarimetric Parameters and Optical Spectral Vegetation Indices Selection

Based on published literature and the sensitivity of optical and polarization features to LAI and biomass, radar polarimetric parameters and optical spectral vegetation indices were used to estimate LAI and biomass. In this study, radar polarimetric parameters (HH, HV, VV, HH/VV, HH/HV,

VV/HV, Vol/Span, Dbl/Span, Odd/Span, and radar vegetation index (RVI)) [48] and optical vegetation indices (Table 5 [18,49–53]) (ratio vegetation index (RVI1), normalized difference vegetation index (NDVI), soil adjusted vegetation index (SAVI), optimized soil adjusted vegetation index (OSAVI), enhanced vegetation index (EVI), and modified triangular vegetation index (MTVI2)) were selected to analyze the relationships between vegetation indices and LAI, biomass.

Table 5. Summary of selected optical vegetation indices used in this study and citations for LAI and biomass.

Vegetation Index	Abbreviation	Formula	Reference
Ratio vegetation index	RVI1[#]	R_{NIR}/R_R	[49]
Normalized Difference Vegetation Index	NDVI	$(R_{NIR} - R_R)/(R_{NIR} + R_R)$	[50]
Soil adjusted vegetation index	SAVI	$(1 + L)(R_{NIR} - R_R)/(R_{NIR} + R_R + L)$; L = 0.5	[51]
Optimized soil adjusted vegetation index	OSAVI	$(R_{NIR} - R_R)/(R_{NIR} + R_R + 0.16)$	[52]
Enhanced Vegetation Index	EVI	$2.5(R_{NIR} - R_R)/(1 + R_{NIR} + 6R_R - 7.5 \times R_B)$	[53]
Modified triangular vegetation index 2	MTVI2	$\frac{1.5[1.2(R_{NIR} - R_G) - 2.5(R_R - R_G)]}{\sqrt{(2R_{NIR}+1)^2 - (6R_{NIR} - 5\sqrt{R_R} - 0.5)}}$	[18]

Note: # Named by this study; R_i denotes reflectance at band i (nanometer). R_B represents reflectance of blue band of HJ-CCD, R_G represents reflectance of green band of HJ-CCD, R_R represents reflectance of red band of HJ-CCD, R_{NIR} represents reflectance of near infrared band of HJ-CCD.

2.5. Method

In this study, firstly, the relationships of parameters with LAI and biomass were examined using linear and nonlinear regression analysis. The parameters of the satellite images included the optical spectral vegetation indices (OSVIs) of HJ-1A/B and the radar polarimetric parameters (RPPs) of RADARSAT-2. Secondly, LAI and biomass were estimated with combined OSVIs and RPPs (the product of OSVIs and RPPs (COSVI-RPPs)). Finally, the COSVI-RPPs were used to estimate the LAI and biomass with multiple stepwise regression (MSR) and partial least squares regression (PLSR) methods. The MSR combines a forward selection and backward elimination. At each step, the best remaining variable was added, provided it passed the significant at 5% criterion test. Then all variables in the regression were checked to see if any could be removed, using the greater than 10% significance criterion. The process continued until no more variables could be added or removed. The remaining regression was used for further analysis [54]. The PLSR is an extension of the multiple linear regression model (e.g., multiple regression or general stepwise regression). This method is particularly useful when one needs to predict a set of dependent variables from a (very) large set of independent variables. In its simplest form, a linear model specifies the (linear) relationship between a dependent (response) variable y and a set of predictor variables [55], the x variables, so that

$$y = b_0 + b_1x_1 + b_2x_2 + b_3x_3 + \ldots + b_px_p \quad (1)$$

In this equation, b_0 is the regression coefficient for the intercept, and the b_i values are regression coefficients (for variables 1 to p) computed from the data.

2.6. Statistical Analysis

The coefficient of determination (R^2), root mean square error (RMSE), and normal RMSE (nRMSE) between LAI and biomass and the OSVIs, RPPs, and COSVI-RPPs were analyzed and used to indicate the main relationships between these five groups of data. The R^2, RMSE, and nRMSE were used to quantify the amount of variation explained by the developed relationships, as well as the accuracy of the relationships. The R^2, RMSE, and nRMSE were used to sort out the regression equation from a series of tested relationships. Sometimes, it is difficult to compare linear and nonlinear relationships with R^2 values. The RMSE and nRMSE can be used to better judge the quality of the estimation model with the exception of R^2. In our study, the RMSE and nRMSE values were more strongly considered than the R^2 value. Finally, we comprehensively considered these statistical criteria to select the best fitting regression equation for estimating LAI and biomass in winter wheat. Generally, the performance of the model was estimated by comparing the differences in the predictions of R^2, RMSE, and nRMSE. The model with higher R^2 values and corresponding lower RMSE and nRMSE values [56] was selected to estimate winter wheat LAI and biomass.

3. Results

3.1. Relationships between Optical Spectral Vegetation Indices and LAI, Biomass

Linear and nonlinear regression analysis was investigated using optical spectral vegetation indices (OSVIs) as the independent variable, and the LAI and biomass of winter wheat as the dependent variable. Six OSVIs were selected based on previous literature. Good relationships between the OSVIs and LAI, biomass were measured and the regression equations of LAI and biomass were built for winter wheat (Table 6). To find the more sensitive OSVIs, we analyzed the OSVIs behavior with respect to the R^2 values. Table 6 showed that the regression relationships between the VIs and LAI, biomasses were significant. RVI1 and MTVI2 had the lowest and highest R^2 values (0.38 and 0.58, respectively) for winter wheat LAI. The order of the indices from highest to lowest with respect to the R^2 values for the LAI regression was MTVI2, EVI, OSAVI, SAVI, NDVI, and RVI1. The R^2 values of MTVI2, EVI, OSAVI, SAVI, NDVI, and RVI1 were 0.58, 0.50, 0.43, 0.43, 0.39, and 0.38, respectively. Of the R^2 values, one was above 0.50, three were above 0.4, and two were below 0.4. The relationship between biomass and VIs behaved similarly to the relationship between LAI and OSVIs (Table 6). However, the R^2 of these relationships were different. The highest and lowest regression relationships were EVI and RVI1 for biomass. For the LAI regression, the MTVI2, EVI, SAVI, and RVI1 were fitted to power equations, whereas OSAVI was fitted to the linear equation. In contrast, all of the OSVIs were fitted to power equations for biomass.

To validate the estimation accuracy of LAI and biomass, the predicted values and the measured values were compared based on their RMSE and nRMSE values. The results showed that the RMSE values ranged from 0.70 to 0.89 and the nRMSE values from 21.02% to 26.69% for LAI; the RMSE values ranged from 198.65 g/m^2 to 337.35 g/m^2 and the nRMSE values from 27.44% to 46.46% for biomass (Table 6).

Table 6. The regression relationships between optical spectral vegetation indices and winter wheat LAI, biomass (n = 80).

Vegetation Indices	LAI				Biomass			
	Regression Equations	R^2	RMSE	nRMSE (%)	Regression Equations	R^2	RMSE (g/m^2)	nRMSE (%)
RVI1	$y = 1.3573x^{0.7615}$	0.38 **	0.77	23.21	$y = 77.178x^{1.596}$	0.51**	337.35	46.61
NDVI	$y = 1.1151e^{2.1763x}$	0.39 **	0.89	26.69	$y = 2898.2x^{2.401}$	0.55**	306.40	42.34
SAVI	$y = 7.317x^{0.8061}$	0.43 **	0.73	21.92	$y = 2613.8x^{1.6528}$	0.58**	267.25	36.95
OSAVI	$y = 6.5324x + 0.9519$	0.43 **	0.80	24.02	$y = 2573.2x^{1.696}$	0.62**	245.63	33.93
EVI	$y = 6.2125x^{0.8524}$	0.50 **	0.72	21.49	$y = 1867.4x^{1.7007}$	0.68**	198.65	27.44
MTVI2	$y = 5.8067x^{0.4841}$	0.58 **	0.70	21.02	$y = 1397.6x^{0.8554}$	0.63**	227.41	31.42

Note: ** Model significant at the 0.01 probability level ($p < 0.01$).

3.2. Relationships between Radar Polarimetric Parameters and LAI, Biomass

Fifteen radar polarimetric parameters (RPPs) were used to study the correlations between RPPs and LAI, biomass. The best and worst RPPs with respect to correlation with LAI were RVI ($R^2 = 0.63$) and Odd/Span ($R^2 = 0.01$), respectively (Table 7). The results showed that the DERD, RVI and HH were highly correlated with LAI. In comparison, the RPPs with the highest and lowest correlations with biomass were DERD ($R^2 = 0.71$) and Odd/Span ($R^2 = 0.01$), respectively (Table 7). All RPPs were well correlated with biomass, with the exception of Dbl/Span and Odd/Span. The relationships between the RPPs and biomass were higher than those between the RPPs and LAI. In particular, the RVI and DERD indices had the highest correlations with LAI and biomass, respectively.

Table 7. The regression relationships between radar polarimetric parameters and winter wheat LAI, biomass (n = 80).

Vegetation Indices	LAI				Biomass			
	Regression Equations	R^2	RMSE	nRMSE (%)	Regression Equations	R^2	RMSE (g/m^2)	nRMSE (%)
Entropy	$y = 7.5432x - 1.3889$	0.36**	1.05	31.53	$y = 2515.2x - 988.45$	0.42**	297.38	41.09
Anisotropy	$y = 1.5255\ln(x) + 5.4445$	0.37**	1.04	31.23	$y = 1534.3x^{0.9401}$	0.44**	302.45	41.79
Alpha	$y = 0.3491x^{0.6558}$	0.33**	1.06	31.83	$y = 1.7927x^{1.6506}$	0.51**	288.62	39.88
SERD	$y = 0.6849e^{2.3616x}$	0.38**	1.21	36.33	$y = 1949.4x^{3.3077}$	0.58**	265.01	36.31
DERD	$y = 1.5644e^{1.3671x}$	0.53**	0.91	27.35	$y = 116.04e^{2.7989x}$	0.71**	164.21	22.70
RVI	$y = 0.7202e^{2.4857x}$	0.63**	0.70	21.02	$y = 2518.5x^{2.8948}$	0.68**	176.52	24.39
HH	$y = 13.072x + 1.6461$	0.52**	0.99	29.73	$y = 4279.6x + 21.069$	0.63**	204.82	28.30
VV	$y = 12.064x + 2.6551$	0.22**	2.94	88.28	$y = 4312x + 301.59$	0.27**	343.25	47.43
HV	$y = 4.1333e^{-6.021x}$	0.10**	3.23	96.99	$y = 978.93e^{-25.4x}$	0.11**	407.14	56.26
HH/VV	$y = 0.4147x + 2.4973$	0.46**	0.96	28.83	$y = 133.7x + 261.98$	0.57**	234.24	32.37
HH/HV	$y = 1.3621\ln(x) + 0.9885$	0.42**	1.01	30.33	$y = 108.73x^{0.8142}$	0.56**	258.62	35.73
VV/HV	$y = 2.2514x^{0.2808}$	0.29**	1.09	32.73	$y = 180.22x^{0.6895}$	0.51**	332.02	45.88
Vol/Span	$y = 5.0295x + 0.8625$	0.37**	1.10	33.03	$y = 998.53\ln(x) + 1272.7$	0.44**	356.12	49.20
Dbl/Span	$y = 0.3357\ln(x) + 4.8477$	$0.03^{n.s.}$	3.48	104.50	$y = 430.17e^{3.9395x}$	$0.03^{n.s.}$	492.46	68.05
Odd/Span	$y = 3.913x^{0.0228}$	$0.01^{n.s.}$	3.64	109.30	$y = 439.07e^{5.5937x}$	$0.01^{n.s.}$	596.32	82.40

Note: Probability levels are indicated by n.s. and ** for "not significant" and $p < 0.01$, respectively.

To validate the estimation accuracy of the regression model, the experimental data (n = 40) was used to compare the predicted LAI and biomass with the measured LAI and biomass. Correlations between the predicted and measured LAI were observed for the following parameters: RVI, DERD, HH/VV, HH, HH/HV, Anisotropy, Entropy, Alpha, VV/HV, Vol/Span, SERD, VV, HV, Dbl/Span, and Odd/Span (Table 7). Similarly, correlations between the predicted and measured biomass were revealed for the following parameters: DERD, RVI, HH, HH/VV, HH/HV, SERD, Alpha, Entropy, Anisotropy, VV/HV, VV, Vol/Span, HV, Dbl/Span, and Odd/Span.

3.3. Relationships of Combined Optical Spectral Vegetation Indices and Radar Polarimetric Parameters with Biomass and LAI

Based on the correlations (R^2) between the RPPs and the LAI and biomass from the field experiment, the RPPs that were best correlated with LAI and biomass were RVI ($R^2 = 0.63$) and DERD ($R^2 = 0.71$). Thus, these indices were used to establish the combined optical spectral vegetation indices and radar polarimetric parameters (COSVI-RPPs) by multiplying each with optical spectral vegetation indices (RVI × OSVIs and DERD × OSVIs). In this study, six OSVIs were individually combined with RVI and with DERD to analyze the relationships of these COSVI-RPPs with LAI and biomass (Table 8). Further, we used these correlations to establish LAI and biomass regression equations for winter wheat. The results revealed that of the R^2 values for the LAI and COSVI-RPPs regressions, one was above 0.65, five were above 0.60, five were below 0.60, and two were equal to 0.60. Of the R^2 values for the biomass and COSVI-RPPs regressions, one was equal 0.80, twelve were above 0.7, and eight were above 0.75. The highest R^2 value was the MTVI2 × RVI ($R^2 = 0.68$) and the lowest was the RVI1 × RVI ($R^2 = 0.56$) for winter wheat LAI. In contrast, the highest R^2 was the EVI × RVI ($R^2 = 0.80$) and the lowest was the RVI1 × DERD ($R^2 = 0.71$) for winter wheat biomass. The results demonstrated that the COSVI-RPPs were highly significantly related to LAI and biomass. They could be used to estimate LAI and biomass in winter wheat. The results show that the MTVI2 × RVI regression equation for estimating LAI and the EVI × RVI regression equation for estimating biomass were fitted to power regression equations (Table 8).

To validate the estimation accuracy of the regression equations for LAI and biomass, the predicted values and the measured values were compared based on the RMSE and nRMSE. The results showed that the RMSE and nRMSE values ranged from 0.65 to 0.80 and 19.52% to 24.02% for LAI, respectively; the RMSE and nRMSE values ranged from 146.33 g/m^2 to 201.47 g/m^2 and 20.21% to 27.84% for biomass, respectively (Table 8). There was good consistency between the predicted values and the measured values. The RMSE and nRMSE values for the regressions between the MTVI2 × RVI and LAI were 0.65 and 19.52%, and those for the regressions between the EVI × RVI and biomass were 146.33 g/m^2 and 20.21%, respectively. The results showed that MTVI2 × RVI and EVI × RVI were better than RVI, MTVI2 and EVI, RVI alone for estimation of LAI and biomass in winter wheat, respectively (Figure 3). The results suggested that the MTVI2 × RVI and EVI × RVI could be used to improve the estimation accuracy of LAI and biomass, respectively.

Table 8. The regression relationships between combined optical spectral vegetation indices and radar polarimetric parameters and winter wheat LAI, biomass (n = 80).

Vegetation Indices	LAI				Biomass			
	Regression Equations	R^2	RMSE	nRMSE (%)	Regression Equations	R^2	RMSE (g/m^2)	nRMSE (%)
RVI1 × RVI	$y = 2.1548x^{0.6209}$	0.56**	0.70	20.72	$y = 231.5x^{1.2164}$	0.72**	182.42	25.20
NDVI × RVI	$y = 1.4685e^{2.4896x}$	0.58**	0.75	22.52	$y = 3217.6x^{1.4544}$	0.77**	151.27	20.90
SAVI × RVI	$y = 8.0998x^{0.6071}$	0.60**	0.68	20.46	$y = 3186.5x^{1.2003}$	0.76**	168.31	23.26
OSAVI × RVI	$y = 8.1476x^{0.6233}$	0.61**	0.74	22.22	$y = 3163.9x^{1.2232}$	0.77**	155.65	20.51
EVI × RVI	$y = 6.9326x^{0.5973}$	0.64**	0.67	20.12	$y = 2394.4x^{1.1858}$	0.80**	146.33	20.21
MTVI2 × RVI	$y = 6.2472x^{0.3814}$	0.68**	0.65	19.52	$y = 1816.2x^{0.7426}$	0.75**	170.58	23.57
RVI1 × DERD	$y = 2.037e^{0.2308x}$	0.52**	0.75	22.52	$y = 190.5e^{0.4714x}$	0.71**	201.47	27.84
NDVI × DERD	$y = 1.8016e^{1.992x}$	0.56**	0.80	24.02	$y = 151.66e^{4.1117x}$	0.79**	159.52	22.04
SAVI × DERD	$y = 1.9088e^{2.2375x}$	0.58**	0.70	20.72	$y = 174.92e^{4.4701x}$	0.76**	161.21	22.28
OSAVI × DERD	$y = 1.896e^{2.2107x}$	0.60**	0.72	21.62	$y = 171.94e^{4.404x}$	0.79**	148.65	20.54
EVI × DERD	$y = 1.848e^{1.8344x}$	0.62**	0.78	23.42	$y = 171.25e^{3.5926x}$	0.78**	156.67	21.65
MTVI2 × DERD	$y = 6.1902x + 2.0154$	0.67**	0.68	20.46	$y = 1781.2x + 216.35$	0.72**	178.43	24.65

Note: ** Model significant at the 0.01 probability level ($p < 0.01$).

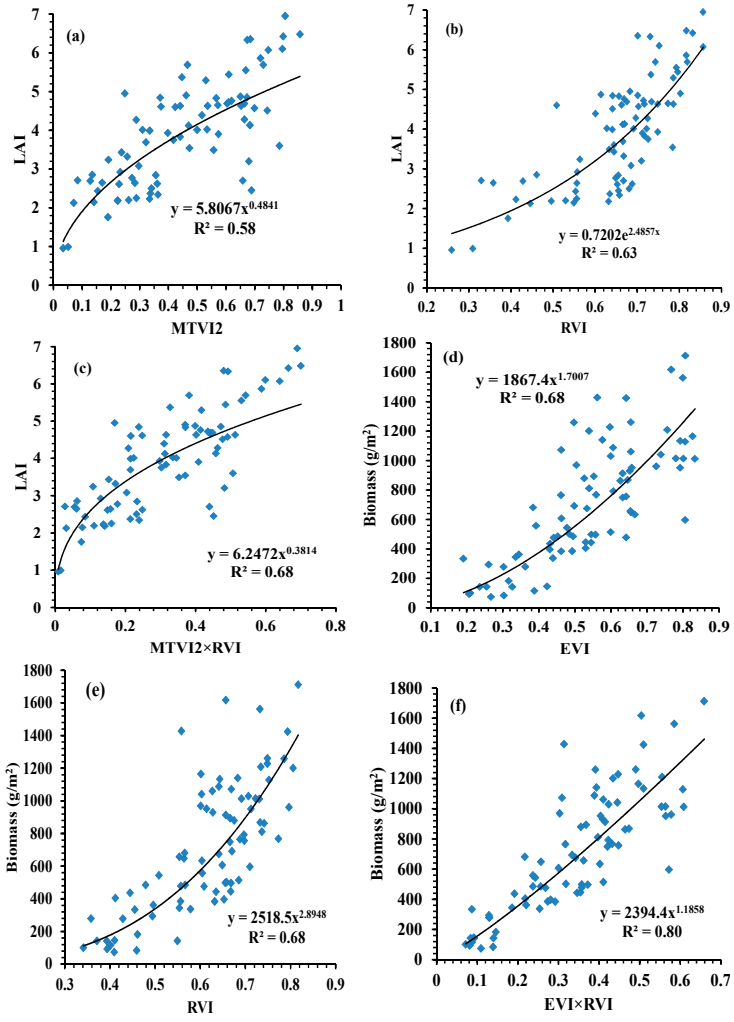

Figure 3. Comparison of MTVI2 (**a**) RVI (**b**) and MTVI2×RVI (**c**) for estimation of LAI and EVI (**d**), RVI (**e**) and EVI×RVI (**f**) for estimation of biomass, respectively.

3.4. Estimation of LAI and Biomass Using Multiple Stepwise Regression (MSR) and Partial Least Squares Regression (PLSR) Methods

The MSR and PLSR methods were used to estimate LAI and biomass for winter wheat based on the COSVI-RPPs, OSVIs, and RPPs. The LAI values were estimated from MSR and PLSR regression equations obtained based on all the COSVI-RPPs, which had R^2 values of 0.73 and 0.76, respectively. Similarly, the biomass values were estimated from MSR and PLSR regression equations and the R^2 values were 0.81 and 0.85, respectively (Table 9). All the COSVI-RPPs, OSVIs, and RPPs were selected as variables to estimate LAI using MSR and PLSR, and the R^2 values of the regression equation were 0.74 and 0.78, respectively. The R^2 of the MSR and PLSR biomass models based on all the COSVI-RPPs, OSVIs, and RPPs were 0.83 and 0.87, respectively.

Table 9. Comparison of multiple stepwise regression and partial least squares regression methods for estimating LAI and biomass of winter wheat based on OSVIs, RPPs, and COSVI-RPPs (n = 80).

Methods	LAI				Biomass			
	Variables	R^2	RMSE	nRMSE (%)	Variables	R^2	RMSE (g/m^2)	nRMSE (%)
Multiple Stepwise regression	EVI × RVI, MTVI2 × DERD	0.73**	0.64	19.22	SAVI × RVI, OSAVI × DERD, MTVI2 × DERD	0.81**	142.63	19.71
Partial least squares regression	12 COSVI-RPPs	0.76**	0.61	18. 31	12 COSVI-RPPs	0.85**	137.21	18.96
Multiple stepwise regression	EVI, DERD, EVI × RVI, MTVI2 × DERD	0.74	0.63	18.92	MTVI2, DERD, SAVI × RVI, OSAVI × DERD, MTVI2 × DERD,	0.83**	140.34	19.39
Partial least squares regression	12 COSVI-RPPs, 6 OSVIs, 15 RPPs	0.78	0.58	17.42	12 COSVI-RPPs, 6 OSVIs, 15 RPPs	0.87**	134.68	18.61

Note: ** Model significant at the 0.01 probability level ($p < 0.01$).

To validate the regression equations, the predicted values obtained from the MSR and PLSR regression equations were compared with the measured values acquired during the entire growth season of winter wheat (n = 40). The results showed that the predicted LAI values were in good agreement with the measured LAI values (Figure 4). RMSEs values of 0.64 and 0.61 and nRMSEs values of 19.22% and 18.13% for LAI were obtained ffrom the MSR and PLSR models based on all the COSVI-RPPs, respectively (Table 9). The RMSEs and nRMSE of the LAI model based on all the COSVI-RPPs, OSVIs, and RPPs using MSR and PLSR were 0.63 and 0.58 and 18.92% and 17.42%, respectively. Furthermore, the results revealed a good relationship between predicted and measured biomass (Figure 5). For the biomass values estimated based on all the COSVI-RPPs using the MSR and PLSR regression equations, the RMSEs were 142.63 g/m^2 and 137.21 g/m^2 and the nRMSEs were 19.71% and 18.96%, respectively (Table 9). RMSEs values of 140.34 g/m^2 and 134.68 g/m^2 and nRMSEs values of 19.39% and 18.61% from the MSR and PLSR biomass models were obtained based on all the COSVI-RPPs, OSVIs, and RPPs, respectively (Table 9). The results showed that the

estimation accuracy of LAI and biomass was higher when obtained by the PLSR than by the MSR equations. Our results indicated that the MSR and PLSR could be used to further improve the estimation accuracy of LAI and biomass for winter wheat.

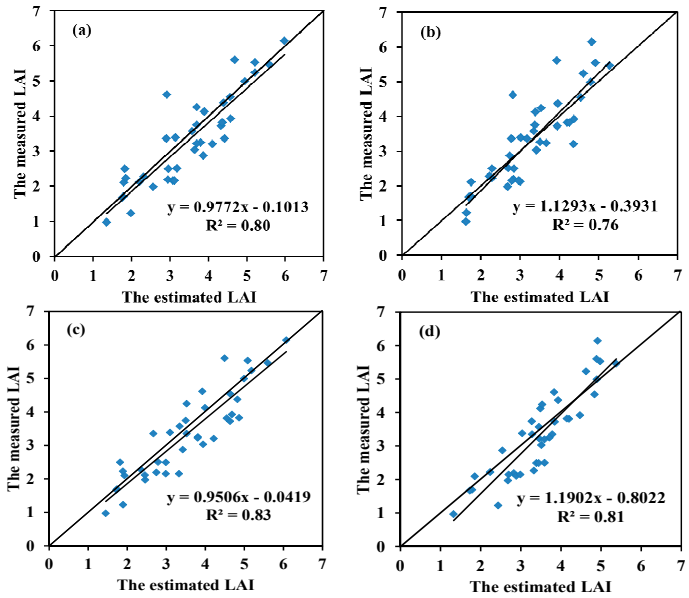

Figure 4. Relationships between predicted LAI and measured LAI of winter wheat: (**a**) partial least squares regression based on all COSVI-RPPs, (**b**) multiple stepwise regression based on all COSVI-RPPs, (**c**) partial least squares regression based on all COSVI-RPPs, OSVIs, and RPPs, (**d**) multiple stepwise regression based on all COSVI-RPPs, OSVIs, and RPPs.

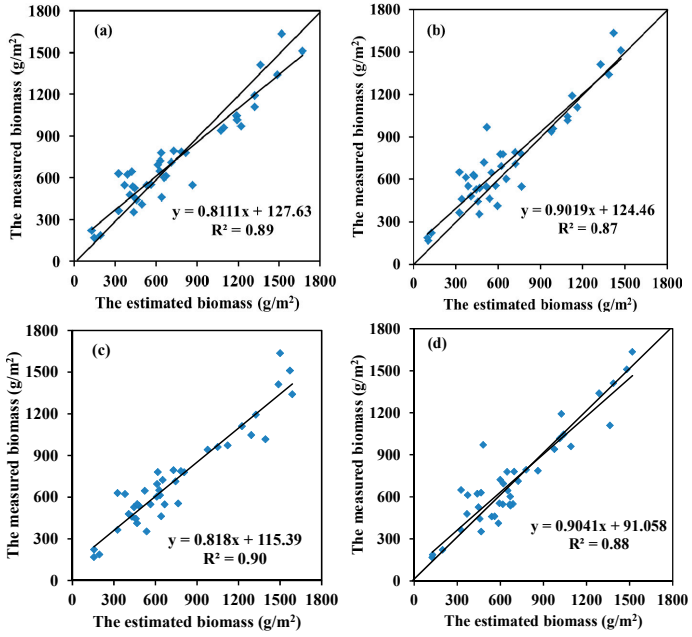

Figure 5. Relationships between predicted biomass and measured biomass of winter wheat: (**a**) partial least squares regression based on all COSVI-RPPs, (**b**) multiple stepwise regression based on all COSVI-RPPs, (**c**) partial least squares regression based on all COSVI-RPPs, OSVIs, and RPPs, (**d**) multiple stepwise regression based on all COSVI-RPPs, OSVIs, and RPPs.

4. Discussion

In this study, six optical spectral vegetation indices (OSVIs) were used to analyze the relationships of OSVIs with LAI and biomass for estimating LAI and biomass in winter wheat. The results showed that OSVIs were correlated with LAI and biomass (Table 6). The effects of LAI and biomass on crop canopy spectral reflectance in the NIR and visible spectrum are known [10–17]. Therefore, these OSVIs based on different combinations of visible and NIR reflectance was significantly related with LAI and biomass. The results of our study confirmed previous results [13–17]. The results showed that MTVI2 and EVI more accurately estimate LAI and biomass than other OSVIs. In addition to the red and NIR bands, EVI includes the blue band, which was used to correct for aerosol influences in the red band. Furthermore, the EVI is an optimized index designed to enhance the vegetation signal with improved sensitivity in high biomass regions through decoupling of the canopy background signal and a reduction in atmospheric and soil background noise influences [53]. Therefore, EVI improves the estimation accuracy of LAI and biomass. The MTVI2 includes the green, red, and NIR bands. The decrease or increase in these bands reflectance influences the total area of the triangle, which was highly related with LAI [18]. In order to reduce soil contamination effects, a soil adjustment factor is incorporated into MTVI2. The results of Haboudane *et al.* [18] indicated that MTVI2 was more sensitive to medium–high LAI. Therefore, the MTVI2 was used to boost the estimation accuracy of LAI and biomass. The results indicated that the EVI and MTVI2 could be used to estimate LAI and biomass in winter wheat. The results of OSVIs showed that the least-correlated with LAI and biomass was RVI1. Our results were consistent with the study of Gao *et al.* [24]. In contrast, OSAVI, SAVI, and NDVI were very sensitive to low LAI (LAI < 3) and were saturated at medium to high LAI values (LAI > 3) [16,50–52]. In this study, most of the LAI values were higher than 3. Therefore, MTVI2 and EVI were better than OSAVI, SAVI, and NDVI for estimating LAI and biomass. These results suggested that the OSVIs could be used to estimate LAI and biomass in winter wheat.

Fifteen radar polarimetric parameters (RPPs) were used to analyze the relationships between LAI, biomass and RPPs. The results showed that good correlations existed with the exception of the Dbl/Span and Odd/Span. The RVI and DERD indices exhibited the strongest correlations with LAI and biomass (Table 7). The results of Koay *et al.* [57] suggested that the increase in HH during the tillering to filling stages was the main reason for the increase in single-volume backscattering as rice canopy became much denser. However, the denser paddy plants canopy showed more vertically oriented scatter, which led to a gradual reduction in the VV from the tillering to filling stages. As for HV, the double-volume scattering is the dominant scattering source at four winter wheat growth stages. The RVI not only included HH, HV, VV, backscattering difference information and then was sensitive to crops structure, but also reduced the environmental and incidence angle effects [48,58]. Therefore, the RVI showed higher correlations with LAI and biomass. The DERD are derived from the eigen-decomposition of the coherency matrix considering the reflection symmetry hypothesis. The results of Allain *et al.* [47] indicated that DERD provides a better inversion of crop parameters in their natural environment because it is easier to discriminate the different scattering mechanisms and eliminate the additive noise term for reducing the biases over the sample eigenvalues. Hence DERD was highly correlated with LAI and biomass. The HH, HV, VV, HH/VV, HH/HV, and VV/HV indices were strongly correlated with LAI and biomass. Previous studies have found that polarization ratios

(HH/VV, HH/HV, and VV/HV) and backscattering coefficients (HH, HV, and VV) are suitable for LAI and biomass estimations in some crops and forests [9,24,36]. Our results were in agreement with these studies. As alpha, anisotropy, and entropy were used to identify the scattering type and its relevance [46], these indices were well correlated with LAI and biomass. The reason Vol/Span was correlated with LAI and biomass was because LAI and biomass largely influenced the range of the Vol change. Gao *et al.* [24] also indicated that Vol had a strong relationship with LAI and biomass. Our results further confirmed theirs results. The values of Odd and Dbl changed little and irregularly in the study of Gao *et al.* [24] and in our results. Therefore, Odd/Span and Dbl/Span were not correlated with LAI or biomass. The results indicated that the most of the RPPs were suitable for estimating LAI and biomass in winter wheat.

Because the NIR reflectance was not sensitive to the LAI or biomass of winter wheat at medium to high LAI, most of the OSVIs demonstrated the saturation phenomenon. However, SAR has some advantages for estimating LAI and biomass at medium to high LAI and biomass [58], and therefore, RPPs were introduced in our study in combination with multispectral data. Previous studies have combined OSVIs and RPPs to estimate biomass and LAI in crops or forests by simply multiplying them [12,24,35,36]. Their results indicated that this method can be used to improve the estimation accuracy of biomass and LAI. Therefore, we combined the optical spectral vegetation indices and radar polarimetric parameters to estimate biomass and LAI in winter wheat by simply multiplying them. The combined indices RVI × OSVIs and DERD × OSVIs were created based on the good relationships between LAI, biomass and OSVIs, RPPs. Compared with the OSVIs and RPPs alone, the results showed that the COSVI-RPPs were more suitable to estimate biomass and LAI at medium to high vegetation coverage. The values of R^2 were 0.68 for LAI and 0.80 for biomass, respectively (Table 8). The better performances of the COSVI-RPPs were attributed to the stronger penetration ability of SAR. The good consistency between the predicted values and measured values was due to the facts that OSVIs can provide an accurate interpretation of crop LAI and biomass and RPPs are more sensitive to crop canopy structure. Both of these factors contributed to the improved estimations of LAI and biomass. The results indicated that the advantages of optical and radar data were integrated and then could be used to enhance their application value. It had great significance to promote the development and integration of optical and radar technology. The results revealed that EVI × RVI and MTVI2 × RVI could be used for robust estimates of LAI and biomass in winter wheat, and the other combined indices were also valuable (Table 8). The result of Capodici *et al.* [27] was also confirmed by our study. In this study, the COSVI-RPPs were acquired according to the spectral reflectance and SAR backscattering mechanism information. These new combined indices were used to estimate canopy structural information (LAI and biomass). The new combined indices were better than the OSVIs and RPPs alone, but more investigations and validations are needed before their regional applications. In this study, the acquisition time had affected the HJ and radar data. The LAI and biomass changed little during the tillering (4 March and 5 March) and filling stages (16 May and 20 May). The difference in the HJ and radar data acquisition time was ignored. However, because LAI and biomass changed at the jointing and anthesis stages, the difference in the HJ and radar data acquisition time may have led to some estimation errors. In particular, winter wheat grows quickly during the jointing stage. The data acquisition time of HJ on April 7th and of the radar data on March 29th resulted in a reduction in the estimation accuracy of LAI and biomass. Therefore, we think that

growth stages impacted the predictive power of the indices, as the plants show very different optical-chemical and structural properties at different growth stages. These differences should influence the optical and SAR signals during different growth stages. Therefore, the small difference in the HJ and radar data acquisition time should be considered to better estimate LAI and biomass in future research. The establishment of regression equations and experimental field data are necessary, and some important factors should be carefully considered in the data analysis. For example, the incidence angle of SAR largely influenced the vegetation backscattering information [27,36] and SAR backscattering information was influenced by the amount of precipitation. These factors may result in some errors in the estimation of water-related crop or soil parameters.

The results of the MSR and PLSR methods show that the COSVI-RPPs were highly related to LAI and biomass of winter wheat (Table 9). The estimation accuracy of LAI and biomass was higher with the PLSR than the MSR method. Previous studies have shown that PLSR outperforms MSR in estimating biophysical and biochemical parameters [11,59]. This may be because the MSR method can be used to concentrate on some spectral band features with known links to the variables of interest [59]. In comparison, the PLSR method fully considered the relationships between the covariance of spectral band features and biophysical variables by applying data compression into regression factors. Therefore, the PLSR obtained the best estimation accuracy of LAI and biomass. However, the MSR also has merit, particularly when taking into consideration the simplicity of its application. But the MSR and PLSR regression models are quite unstable when they are applied to the larger region even though the calibration results look good in our study. Therefore, the performance of MSR and PLSR regression models have to be carefully verified by using sufficient independent datasets of different crops and ecological regions, as this study was limited to winter wheat in the Yangling district of Shaanxi, China.

5. Conclusion

In this study, the optical spectral vegetation indices (OSVIs), radar polarimetric parameters (RPPs), combined optical spectral vegetation indices and radar polarimetric parameters (the product of optical spectral vegetation indices and radar polarimetric parameters (COSVI-RPPs)), and multiple stepwise regression (MSR) and partial least squares regression (PLSR) methods were investigated to determine the most accurate empirical regression equations for LAI and biomass estimation in winter wheat. The results of this study revealed the following conclusions. Strong relationships existed between LAI, biomass and OSVIs, RPPs, and the OSVIs and RPPs could be used to estimate LAI and biomass in winter wheat based on the relevant regression equations. We found a highly significant correlation between the new COSVI-RPPs (RVI × OSVIs and DERD × OSVIs) and LAI and biomass. The estimation accuracy of LAI and biomass was better using RVI × OSVIs and DERD × OSVIs than using the OSVIs and RPPs values alone. The MSR and PLSR methods were used to estimate LAI and biomass in winter wheat based on the results of the COSVI-RPPs. The results demonstrated that the PLSR regression equations based on the COSVI-RPPs resulted in a better estimation of winter wheat LAI ($R^2 = 0.76$, RMSE = 0.61, and nRMSE = 18.13%) and biomass ($R^2 = 0.85$, RMSE = 137.21 g/m^2, and nRMSE = 18.96%). The MSR regression equations based on the COSVI-RPPs also resulted in good estimations of LAI and biomass of winter wheat. The LAI ($R^2 = 0.78$, RMSE = 0.58, and

nRMSE = 17.42%) and biomass (R^2 = 0.87, RMSE = 134.68 g/m^2, and nRMSE = 18.61%) model obtained the best estimation results based on all the COSVI-RPPs, OSVIs, and RPPs using PLSR.

Acknowledgements

This study was supported by the Natural Science Foundation of China (41471285, 41271345, 41471351), the Beijing Natural Science Foundation (4141001), the Special Funds for Technology Innovation Capacity Building sponsored by the Beijing Academy of Agriculture and Forestry Sciences (KJCX20140417, KJCX20150409), Yangzhou University Excellent Doctoral Foundation. We are grateful to China Meteorological Data Sharing Service System and Canada Weather and Climate Data Service System for environment data collection. We are grateful to staffs for field data collection.

Author Contributions

Xiuliang Jin analysed data and wrote the manuscript; Guijun Yang, Xingang Xu, Chunjiang Zhao, Zhenhai Li and Yubin Lan gave comments, suggestions to the manuscript, and checked the writing; Hao Yang, Haikuan Feng, and Jiaxiao Shen provided data and data acquisition capacity.

Conflicts of Interest

The authors declare no conflict of interest.

References

1. Darvishzadeh, R.; Skidmore, A.; Schlerf, M.; Atzberger, C. Inversion of a radiative transfer model for estimating vegetation LAI and chlorophyll in a heterogeneous grassland. *Remote Sens. Environ.* **2008**, *112*, 2592–2604.
2. Scharf, P.C.; Lory, J.A. Calibrating corn color from aerial photographs to predict side-dress nitrogen need. *Agron. J.* **2002**, *94*, 397–404.
3. Bastiaanssen, W.G.M.; Molden, D.J.; Makin, I.W. Remote sensing for irrigated agriculture examples from research and possible applications. *Agr. Water Manage.* **2000**, *46*, 137–155.
4. Hunsaker, D.J.; Barnes, E.M.; Clarke, T.R.; Fitzgerald, G.J.; Pinter, P.J. Cotton irrigation scheduling using remotely sensed and FAO-56 basal crop coefficients. *Trans. ASAE* **2005**, *48*, 1395–1407.
5. Luedeling, E.; Hale, A.; Zhang, M.; Bentley, W.J.; Dharmasri, L.C. Remote sensing of spider mite damage in California peach orchards. *Int. J. Appl. Earth Obs.* **2009**, *11*, 244–255.
6. Mahlein, A.K.; Oerke, E.C.; Steiner, U.; Dehne, H.W. Recent advances in sensing plant diseases for precision crop protection. *Eur. J. Plant. Pathol.* **2012**, *133*, 197–209.
7. Groten, S.M.E. NDVI-crop monitoring and early yield assessment of Burkina Faso. *Int. J. Remote Sens.* **1993**, *14*, 1495–1515.
8. Mkhabela, M.S.; Bullock, P.; Raj, S.; Wang, S.; Yang, Y. Crop yield forecasting on the Canadian Prairies using MODIS NDVI data. *Agr. Forest Meteorol.* **2011**, *151*, 385–393.
9. Dente, L.; Satalino, G.; Mattia, F.; Rinaldi, M. Assimilation of leaf area index derived from ASAR and MERIS data into CERES-wheat model to map wheat yield. *Remote Sens. Environ.* **2008**, *112*, 1395–1407.

10. Bala, S.K.; Islam, A.S. Correlation between potato yield and MODIS-derived vegetation indices. *Int. J. Remote Sens.* **2009**, *30*, 2491–2507.
11. Li, X.C.; Zhang, Y.J.; Luo, J.H., Jin, X.L.; Xu, Y.; Yang, W.Z. Quantification winter wheat LAI with HJ-1CCD image features over multiple growing seasons. *Int. J. Appl. Earth Obs.* **2015**, *44*, 104–112.
12. Koppe, W.; Gnyp, M.L.; Hennig, S.D.; Li, Fei.; Miao, Y.X.; Chen, X.P., Jia, L.L.; Bareth, G. Multi-temporal hyperspectral and radar remote sensing for estimating winter wheat biomass in the North China Plain. *Photogramm. Fernerkund. Geoinf.* **2012**, *2012*, 281–298.
13. Chen, P.; Tremblay, N.; Wang, J.; Vigneaulta, P. New index for crop canopy fresh biomass estimation. *Spectrosc. Spect. Anal.* **2010**, *30*, 512–517.
14. Liu, J.; Pattey, E.; Miller, J.R.; McNairn, H.; Smith, A.; Hu, B. Estimating crop stresses, aboveground dry biomass and yield of corn using multi-temporal optical data combined with a radiation use efficiency model. *Remote Sens. Environ.* **2010**, *114*, 1167–1177.
15. Liu, J.; Pattey, E.; Jégo, J.R.G. Assessment of vegetation indices for regional crop green LAI estimation from Landsat images over multiple growing seasons. *Remote Sens. Environ.* **2012**, *123*, 347–358.
16. Nguy-Robertson, A.; Gitelson, A.; Peng, Y.; Vina, A.; Arkebauer, T.; Rundquist, D. Green leaf area index estimation in maize and soybean: Combining vegetation indices to achieve maximal sensitivity. *Agron. J.* **2012**, *104*, 1336–1347.
17. Jin, X.L.; Diao, W.Y.; Xiao, C.H.; Wang, F.Y.; Chen, B.; Wang, K.R.; Li, S.K. Estimation of wheat agronomic parameters using new spectral indices. *PLoS ONE* **2013**, *8*, doi:10.1371/journal.pone.0072736.
18. Haboudane, D.; Miller, J.R.; Pattey, E.; Zarco-Tejada, P.J.; Strachan, I.B. Hyper-spectral vegetation indices and novel algorithms for predicting green LAI of crop canopies: Modeling and validation in the context of precision agriculture. *Remote Sens. Environ.* **2004**, *90*, 337–352.
19. Liu, J.; Pattey, E.; Shang, J.; Admira, S.; Jégo, G.; McNairn, H.; Smith, A.; Hu, B.; Zhang, F.; Freementle, J. Quantifying crop biomass accumulation using multi-temporal optical remote sensing observations. In Proceedings of the 30th Canadian Symposium on Remote Sensing, Lethbridge, AB, Canada, 22–25 June 2009.
20. Vina, A.; Gitelson, A.A.; Nguy-Robertson, A.L.; Peng, Y. Comparison of different vegetation indices for the remote assessment of green leaf area index of crops. *Remote Sens. Environ.* **2011**, *115*, 3468–3478.
21. Ramoelo, A.; Skidmore, A.K.; Cho, M.A.; Schlerf, M.; Mathieu, R.; Heitkönig, I.M.A. Regional estimation of savanna grass nitrogen using the red-edge band of the spaceborne RapidEye sensor. *Int. J. Appl. Earth Obs.* **2012**, *19*, 151–162.
22. Tang, S.; Chen, J.M.; Zhu, Q.; Li, X.; Chen, M.; Sun, R.; Zhou, Y.; Deng, F.; Xie, D. LAI inversion algorithm based on directional reflectance kernels. *J. Environ. Manage.* **2007**, *85*, 638–648.
23. Ulaby, F.; Moore, R.; Fung, A. *Microwave Remote Sensing: From Theory to Applications*; Artech House Publishers: Norwood, MA, USA, 1986.
24. Gao, S.; Niu, Z.; Huang, N.; Hou, X.H. Estimating the leaf area index, height and biomass of maize using HJ-1 and RADARSAT-2. *Int. J. Appl. Earth Obs.* **2013**, *24*, 1–8.
25. eoPortal Directory. Satellite Missions Database. Available online: https://directory.eoportal.org/web/eoportal/satellite-missions (accessed on 21 August 2015).

26. Global Monitoring for Environment and Security (GMES)-Observing the Earth. Synthetic Aperture Radar Missions. Available online: http://www.esa.int/Our_Activities/Observing_the_Earth/GMES/SAR_missions (accessed on 21 August 2015).
27. Capodici, F.; D'Urso, G.; Maltese, A. Investigating the Relationship between X-Band SAR Data from COSMO-SkyMed Satellite and NDVI for LAI Detection. *Remote Sens.* **2013**, *5*, 1389–1404.
28. Cutler, M.E.J.; Boyd, D.S.; Foody, G.M.; Vetrivel, A. Estimating tropical forest biomass with a combination of SAR image texture and Landsat TM data: An assessment of predictions between regions. *ISPRS J. Photogramm. Remote Sens.* **2012**, *70*, 66–77.
29. Imhoff, M.L. Radar backscatter and biomass saturation: Ramifications for global biomass inventory. *IEEE Trans. Geosci. Remote Sens.* **1995**, *33*, 511–518.
30. Lu, D. The potential and challenge of remote sensing-based biomass estimation. *Int. J. Remote Sens.* **2006**, *27*, 1297–1328.
31. Rauste, Y. Multi-temporal JERS SAR data in boreal forest mapping. *Remote Sens. Environ.* **2005**, *97*, 263–275.
32. Castel, T.; Guerra, F.; Caraglio, Y.; Houllier, F. Retrieval biomass of a large Venezuelan pine plantation using JERS-1 SAR data-Analysis of forest structure impact on radar signature. *Remote Sens. Environ.* **2002**, *79*, 30–41.
33. Lucas, R.M.; Cronin, N.; Lee, A.; Moghaddam, M.; Witte, C.; Tickle, P. Empirical relationships between AIRSAR backscatter and LiDAR-derived forest biomass, Queensland, Australia. *Remote Sens. Environ.* **2006**, *100*, 407–425.
34. Lucas, R.M.; Cronin, N.; Moghaddam, M.; Lee, A.; Armston, J.; Bunting, P.; Witte, C. Integration of radar and Landsat-derived foliage projected cover for woody regrowth mapping, Queensland, Australia. *Remote Sens. Environ.* **2006**, *100*, 388–406.
35. Clevers, J.G.P.W.; Vanleeuwen, H.J.C. Combined use of optical and microwave remote sensing data for crop growth monitoring. *Remote Sens. Environ.* **1996**, *56*, 42–51.
36. Manninen, T.; Smolander, H.; Voipio, P.; Stenberg, P.; Rautiainen, M.; Ahola, H. Boreal forest LAI retrieval using both optical and microwave data of ENVISAT. In Proceedings of the 2005 IEEE International Geoscience and Remote Sensing Symposium, Seoul, Korea, 25–29 July 2005.
37. Kar, G.; Verma, H.N.; Singh, R. Effect of winter crop and supplementary irrigation on crop yield, water use efficiency and profitability in rainfed rice based on cropping system of eastern India. *Agr. Water Manage.* **2006**, *79*, 280–292.
38. Dettwiler, M. *Radarsat-2 Product Format Definition*; Macdonald, Dettwiler and Associates Ltd.: Richmond, BC, Canada, 2008.
39. Koppe, W.; Gnyp, M.L.; Hütt, C.; Yao, Y.; Miao, Y.; Chen, X.; Bareth, G. Rice monitoring with multi-temporal and dual-polarimetric TerraSAR-X data. *Int. J. Appl. Earth Obs.* **2013**, *21*, 568–576.
40. Johnstone, I.M.; Raimondo, M. Periodic boxcar deconvolution and diophantine approximation. *Ann. Stat.* **2004**, *32*, 1781–1804.
41. Lee, J.S.; Pottier, E. *Polarimetric Radar Imaging: From Basics to Applications*; CRC Press: New York, NY, USA, 2009.
42. Sheng, Y.; Alsdorf, D.E. Automated georeferencing and orthorectification of Amazon basin-wide SAR mosaics using SRTM DEM data. *IEEE Trans. Geosci. Remote Sens.* **2005**, *43*, 1929–1940.

43. Gens, R.; Pottier, E.; Atwood, D.K. Geocoding of polarimetric processing results: Alternative processing strategies. *Remote Sens. Lett.* **2013**, *4*, 39–45.
44. Cloude, S.R. *Polarisation: Applications in Remote Sensing*; Oxford University Press: Oxford, UK, 2009.
45. Freeman, A.; Durden, S.L. A three-component scattering model for polarimetric SAR data. *IEEE Trans. Geosci. Remote Sens.* **1998**, *36*, 963–973.
46. Cloude, S.R.; Pottier, E. An entropy based classification scheme for land applications of polarimetric SAR. *IEEE Trans. Geosci. Remote Sens.* **1997**, *35*, 68–78.
47. Allain, S.; Ferro-Famil L.; Pottier, E. A polarimetric classification from POLSAR data using SERD/DERD parameters. In Proceedings of the 6th European Conference on Synthetic Aperture Radar, Dresden, Germany, 16–18 May 2006.
48. Kim, Y.; van Zyl, J.J. Comparison of forest estimation techniques using SAR data. In Proceedings of the 2011 IEEE International Geoscience and Remote Sensing Symposium, Vancouver, BC, Canada, 24–29 July 2011; pp. 1395–1397.
49. Birth, G.S.; McVey, G. Measuring the color of growing turf with a reflectance spectroradiometer. *Agron. J.* **1968**, *60*, 640–643.
50. Rouse, J.W., Jr.; Haas, R.H.; Schell, J.A.; Deering, D.W.; Harlan, J.C. *Monitoring the Vernal Advancement of Retrogradation (Green Wave Effect) of Natural Vegetation*; Texas A & M University: Greenbelt, MD, USA, 1974.
51. Huete, A.R. A soil-adjusted vegetation index (SAVI). *Remote Sens. Environ.* **1988**, *25*, 295–309.
52. Rondeaux, G.; Steven, M.; Baret, F. Optimization of soil-adjusted vegetation indices. *Remote Sens. Environ.* **1996**, *55*, 95–107.
53. Liu, H.Q.; Huete, A.R. A feedback based modification of the NDVI to minimize canopy background and atmospheric noise. *IEEE Trans. Geosci. Remote Sens.* **1995**, *33*, 457–465.
54. Jin, X.L.; Wang, K.R.; Xiao, C.H.; Diao, W.Y.; Wang, F.Y.; Chen, B.; Li, S.K. Comparison of two methods for estimation of leaf total chlorophyll content using remote sensing in wheat. *Field Crop. Res.* **2012**, *135*, 24–29.
55. Jin, X.L.; Xu, X.G.; Song, X.Y.; Li, Z.H.; Wang, J.H.; Guo, W.S. Estimation of leaf water content in winter wheat using grey relational analysis–Partial least squares modeling with hyperspectral data. *Agron. J.* **2013**, *105*, 1385–1392.
56. Wang, B.S. *Field-Experiment and Statistic-Method*; China Agriculture Press: Beijing, China, 2002.
57. Koay, J.Y.; Tan, C.P.; Lim, K.S.; Bin Abu Bakar, S.B.; Ewe, H.T.; Chuah, H.T.; Kong, J.A. Paddy fields as electrically dense media: Theoretical modeling and measurement comparisons. *IEEE Trans. Geosci. Remote Sens.* **2007**, *45*, 2837–2849.
58. Karam, M.; Fung, A.; Lang R.; Chauhan, N. A microwave scattering model for layered vegetation. *IEEE Trans. Geosci. Remote Sens.* **1992**, *30*, 767–784.
59. Fourty, T.; Baret, F. Vegetation water and dry matter contents estimated from top-of-the-atmosphere reflectance data: A simulation. *Remote Sens. Environ.* **1997**, *61*, 34–45.

© 2015 by the authors; licensee MDPI, Basel, Switzerland. This article is an open access article distributed under the terms and conditions of the Creative Commons Attribution license (http://creativecommons.org/licenses/by/4.0/).